Polymer 51 (2010) 4713–4725

Contents lists available at ScienceDirect

Polymer

journal homepage: www.elsevier.com/locate/polymer

Supported hybrid early and late transition metal catalysts for the synthesis of polyethylene with tailored molecular weight and chemical composition distributions

Yiyoung Choi, João B.P. Soares*

Department of Chemical Engineering, University of Waterloo, Ontario, Canada N2L 3G1

ARTICLE INFO

Article history:
Received 8 July 2010
Received in revised form
10 August 2010
Accepted 14 August 2010
Available online 21 August 2010

Keywords:
Polyethylene
Supported catalyst
Hybrid catalyst

ABSTRACT

Supported hybrid catalysts using metallocenes and a nickel diimine catalyst were synthesized and used for ethylene slurry polymerization and ethylene/1-hexene copolymerization. Two types of metallocenes, together with a nickel diimine catalyst were supported onto SiO_2 through chemical bonding, and a borate compound was physisorbed for the activation of the catalysts. These supported hybrid catalysts had high catalyst activities and made free-flowing polymer particles. The chemical composition distribution, molecular weight averages and distributions of resultant polymers were controlled by catalyst structure and polymerization conditions such as reaction temperature and the use of α-olefin. According to GPC-IR, ^{13}C NMR and CEF characterization results of some polymers, more 1-hexene was incorporated in the high molecular weight region, short chain branches were generated by the chain walking mechanism in low molecular weight region. The morphologies of the resulting particles were investigated by SEM.

1. Introduction

Metallocenes have been considered as a possible replacement for Ziegler–Natta catalysts for production of linear low-density polyethylene (LLDPE) due to their remarkable α-olefin reactivity. Although LLDPE made with metallocenes offers superior mechanical properties such as excellent toughness, impact strength and clarity, it suffers from poor processability. To overcome this disadvantage, LLDPE may be produced with a bimodal molecular weight distribution (MWD). The advantages of bimodal resins are in the control of the chemical composition distribution (CCD) as well as the MWD. The presence of more short chain branches (SCB) in the higher molecular weight region improves the strength properties and reduces brittleness. This fraction has been linked to the formation of tie molecules between the crystalline lamellae, resulting in improved stress crack resistance, for instance. For the typical industrial production of LLDPE with tailored MWD and SCB distribution (SCBD), serial or cascade reactors are involved, where each reactor produces a polymer with desired properties controlled by the polymerization conditions [1–3].

Alternatively, in order to take advantage of commonly available polymerization plant infrastructure using a single reactor, the use of hybrid catalyst systems, where each catalyst makes a polymer with its own unique properties, has considerable value [3,4]. Obviously, hybrid metallocene catalysts can be selected to make bimodal MWD resins. Because metallocene catalysts produce polymers with narrow MWD and constant SCB averages across the MWD, combining a metallocene that makes high molecular weight polymer with higher co-monomer content and another metallocene that produces low molecular weight polymer with low co-monomer content is an evident way to produce a bimodal product. For example, $Me_2Si(C_5Me_4)(N\text{-}tBu)TiCl_2$ (a constrained geometry catalyst, CGC) has an open structure around the active sites, resulting in olefin copolymer production with high α-olefin content. On the other hand, $(n\text{BuCp})_2ZrCl_2$ makes low molecular polymer with low α-olefin content [3]. Therefore, a hybrid catalyst using CGC/$(n\text{BuCp})_2ZrCl_2$ could make polyethylene with bimodal MWD and reverse co-monomer incorporation. Nevertheless, "optimal" hybrid catalysts are hard to accomplish because each catalyst has its own characteristics, such as life time, activity, co-monomer response, and hydrogen sensitivity. Thus, chemical and kinetic compatibilities must be taken into account to create a well-balanced catalyst useful for industrial plant operation.

Olefin polymerization processes in slurry and gas-phase reactors require the use of solid-supported catalysts. The catalyst should not leach from the support during polymerization, and the catalyst structure, activity, and co-monomer reactivity must be maintained after supporting. For continuous operation of processes with single-site catalysts, this requires fixing soluble catalysts such as early and late

* Corresponding author. Fax: +1 519 746 4979.
E-mail address: jsoares@uwaterloo.ca (J.B.P. Soares).

0032-3861/$ – see front matter © 2010 Elsevier Ltd. All rights reserved.
doi:10.1016/j.polymer.2010.08.030

transition metal complexes onto insoluble carriers [5–9]. Physical-adsorption supporting methods are commonly used for metallocene supporting due to its simplicity [10]. However, metallocenes supported through physical-adsorption can be extracted by diluents during polymerization in slurry reactors. These solubilized sites make polymer particles with poor morphology and may form or cause polymer chunks that lead reactor fouling. In addition, the catalyst active sites may react with impurities on the inorganic carrier or hydroxyl groups on the SiO_2-support surface, producing inactive sites and significantly decreasing catalyst activity. Alternatively, chemical supporting methods create covalent chemical bonds between the catalyst and the support [11–13]. In this method, a functionalized metallocene is synthesized first and then the functional groups on the metallocene ligand are allowed to react with other functional groups present on the support surface. Chemically tethered groups, which are strongly connected between metallocene and support, can reduce catalyst leaching from the support surface, thus minimizing reactor fouling.

Dubois et al. used SiO_2 surface hydroxyl groups to anchor functionalized metallocene complexes [13]. Unfortunately, side reactions may also take place during the supporting process (for example, between other metallocene ligands such as chlorine and SiO_2), forming inactive sites and other byproducts, such as water and hydrochloride acid, that act as catalyst poisons. Repsol introduced a metallocene supporting method where siloxane groups on the SiO_2 surface react with functional groups on the metallocene ligands to create a supported metallocene [14]. This method is attractive because byproducts such as water are not formed during catalyst supporting. Introducing a spacer group between the support surface and the catalyst is considered by some researchers the best method to improve catalyst activity. The spacer group reduces not only electronic, but also steric effects between support and catalyst [15]. LG Chem developed hybrid SiO_2-supported metallocene systems, where a metallocene with functionalized spacer groups led to high catalyst activity and to the production of bimodal ethylene copolymers with controlled microstructures [16]. For supported late transition metal catalysts, SiO_2-supported nickel diimine catalysts, where the catalyst sites had been covalently bonded to the support, are also very active and produce polyethylenes having SCBs without the use of any co-monomer due to the chain walking mechanism. The use of internal borate activators with these systems helps reducing reactor fouling, and obtains spherical polymer particles with good morphology [17].

In this work, we report the synthesis of supported hybrid early and late transition metal catalysts to polymerize ethylene in a slurry reactor. The metallocene is supported on SiO_2 to make high molecular weight polymer with controlled SCBs by addition of 1-hexene. The nickel diimine catalyst is supported on the same SiO_2-support to produce low molecular weight polymer with controllable SCB frequency by the chain walking mechanism. These hybrid catalysts can make polymers with precisely tailored SCBs frequencies, especially inverse SCBDs, as well as broad MWD. The resultant polyethylene particles were spherical and free-flowing, ideally suited for slurry and gas-phase processes. The polymer microstructure was analyzed by high-temperature gel permeation chromatography with infrared spectroscopy detector (GPC-IR), crystallization elution fractionation (CEF), and nuclear magnetic resonance (^{13}C NMR). The polymer particle morphology was characterized by scanning electron microscopy (SEM).

2. Experimental

2.1. Materials

All operations were carried out under high purity nitrogen (99.999%, Praxair) using standard Schlenk techniques or inside a glove box (Vacuum Atmosphere Company, Nexus). Polymer grade ethylene (99.9%, Praxair) and nitrogen were purified by passing through columns packed with R3-11 copper catalyst, activated alumina and 3A/4A mixed molecular sieves. Materials for bis(4-amino-2,3,5,6-tetramethylimino)acenaphtene nickel(II) dibromide (named **N**) synthesis [18] were purchased from Aldrich and used without further purification. The metallocenes, Bis(6-t-butoxyhexylcyclopentadienylide)zirconium dichloride (named **Z**), and methyl (6-t-Butoxyhexyl)silyl(η^5-tetramethylcyclopentadienyl)(t-butylamido)titanium dichloride (named **T**) were provided by LG Chem [16]. The trimethyl aluminums (TMA, 2 M in toluene and in hexane) were purchased from Aldrich. SiO_2 (Sylopol 948, Grace Davison: average particle size 55 μm, total volatiles 10.0%, surface area 280–355 m^2/g, pore volume 1.55 cc/g) was used as the catalyst support after drying under vacuum overnight at 150 °C. Solvents for catalyst synthesis and polymerization were purified by passing through columns packed with activated alumina and molecular sieves (Zeolum Type F-9, Tosoh Co.). The borate activator, dimethylanilium tetrakis(pentafluorophenyl)borate (named **B**) was purchased from Strem Chemicals. The structure of the used catalysts and the borate activator are shown in Fig. 1.

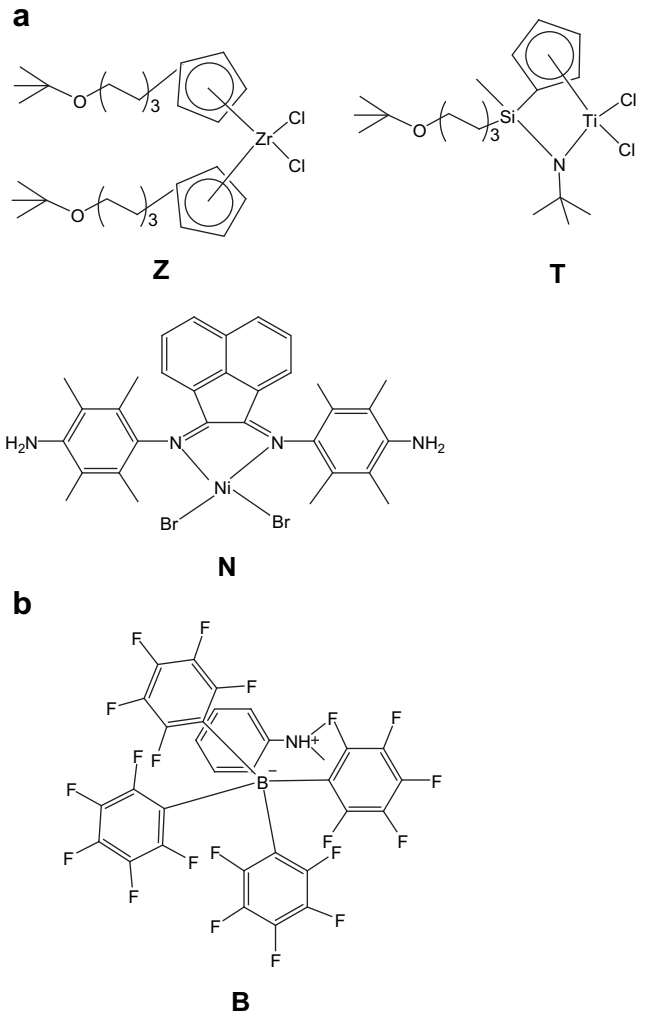

Fig. 1. a) Catalysts: Bis(6-t-butoxyhexylcyclopentadienylide)zirconium dichloride (**Z**), methyl(6-t-Butoxyhexyl)silyl(η^5-tetramethylcyclopentadienyl)(t-butylamido)titanium dichloride (**T**), and bis(4-amino-2,3,5,6-tetramethylimino)acenaphtene nickel(II) dibromide (**N**); and b) Activator: dimethylanilium tetrakis(pentafluorophenyl)borate (**B**).

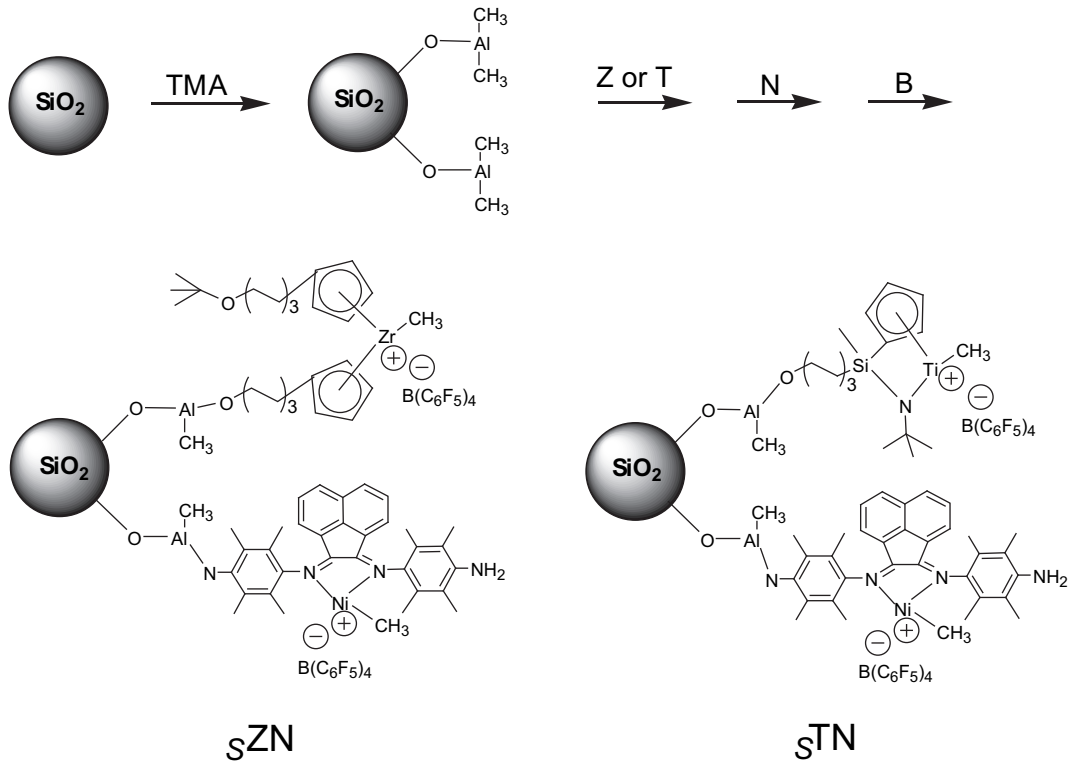

Scheme 1. Synthesis steps for supported hybrid catalysts ($_S$**ZN** and $_S$**TN**).

2.2. Synthesis of supported catalysts

2.2.1. Supported single catalysts ($_S$*N*, $_S$*Z*, $_S$*T*)

One gram of dried Sylopol 948 and 20 mL toluene were introduced in a dried 225 mL glass reactor equipped with a mechanical stirrer (Lab-Crest Glass Pressure Reaction Vessels, Andrews Glass Co.). An amount of 20 mmol TMA (2 M toluene solution) was slowly added to the reactor at 60 °C with a stirring rate of 200 rpm and reacted overnight. After stopping the stirrer, the supernatant liquid was removed with a cannula, the product was washed three times with 20 mL dichloromethane, and finally heated at 30 °C under 200 rpm. An amount of 0.07 mmol **N** was added with 20 mL dichloromethane to the reactor, and reacted overnight. The product was filtered, washed with 20 mL toluene, and heated at 30 °C under 200 rpm. An amount of 0.14 mmol **B** was added to the reactor with 20 mL dichloromethane and reacted for 3 h, then dried under vacuum without washing. This final supported catalyst was named $_S$**N**.

Other supported catalysts using single catalysts, $_S$**Z** and $_S$**T**, were synthesized according to a similar procedure, but toluene was used instead of dichloromethane as solvent.

2.2.2. Supported hybrid catalysts ($_S$*ZN*, $_S$*TN*)

The procedure for making the hybrid catalysts was similar to that used for the single catalysts. After supporting 0.035 mmol of **Z** onto SiO_2, filtering, and washing, 0.035 mmol of **N** was supported following the same procedure, and then 0.14 mmol **B** was added to the support and dried without further treatment. The final supported catalyst was named $_S$**ZN**.

The hybrid catalyst $_S$**TN** was synthesized according to same procedure, but 0.175 mmol of **T** and 0.42 mmol of **B** were used.

2.3. Characterization of the supported catalysts

Zr, Ti, Ni, and Al contents on the supported catalysts were measured by inductively coupled plasma-optical emission spectroscopy (ICP, Teledyne Leeman Labs, Prodigy High Dispersion ICP). A mass of 20 mg of supported catalyst was dissolved in 10 mL 3 N HNO_3 solution. The solution was diluted with distilled water prior to analysis.

2.4. Polymerization

Polymerizations were carried out in a 300 ml semi-batch autoclave reactor, equipped with a mass flow controller and a temperature control unit consisting of a cooling coil and an electric heater. The polymerization temperature was maintained within ± 0.2 °C of the set point. Prior to each polymerization, the reactor was purged several times with nitrogen, then heated to 120 °C under vacuum and purged again with nitrogen to the set point temperature. A volume of 150 mL hexane, 0.1 mmol TMA (2 M hexane solution) as a scavenger, and the desired amount of 1-hexene were transferred to the reactor. As soon as the supported catalyst was introduced in the form of hexane slurry, the polymerization took place under

Table 1
Description of the supported catalysts.

Name	Components			ICP results		Supporting efficiency[a]	
	Catalyst (mmol)	TMA (mmol)	Borate (mmol)	Zr, Ti, Ni (mmol/g catalyst)	Al (mmol/g catalyst)	Zr, Ti, Ni (wt.-%)	Al (wt.-%)
$_S$**Z**	Z 0.07	20	0.14	Zr 0.054	1.421	96.4	14.8
$_S$**T**	T 0.07	20	0.14	Ti 0.053	1.425	92.9	15.0
$_S$**N**	N 0.07	20	0.14	Ni 0.055	1.429	98.2	15.1
$_S$**ZN**	Z 0.035, N 0.035	20	0.14	Zr 0.026, Ni 0.027	1.318	Zr 96.3, Ni 96.3	14.6
$_S$**TN**	T 0.175, N 0.035	20	0.42	Ti 0.101, Ni 0.022	1.420	Ti 91.1, Ni 95.7	14.7

SiO_2-Support: Sylopol 1 g.
[a] Calculated on ICP results of Al deposition, and assumption of 100% borate deposition.

Table 2
Results for ethylene homopolymerization and ethylene/1-hexene copolymerization using supported single catalysts $_S$**Z** and $_S$**T**.

Run	Polymerization Conditions			Results				
	Catalyst	Temperature (°C)	1-hexene (C6/C2)[a]	Yield (g)	Activity[b]	T_m (°C)	M_w (g/mol × 10^{-3})	M_w/M_n
1	$_S$**Z**	40	0	0.8	3250	133.3	382	3.6
2	$_S$**Z**	40	0.2	0.8	2110	128.0	247	3.8
3	$_S$**Z**	40	0.4	0.8	2030	124.7	215	3.1
4	$_S$**Z**	60	0	2.8	11280	134.4	178	3.3
5	$_S$**Z**	60	0.2	2.1	7660	127.0	133	3.0
6	$_S$**Z**	60	0.4	1.3	4750	122.8	118	3.9
7	$_S$**Z**	70	0	4.4	17630	133.0	150	3.9
8	$_S$**Z**	70	0.2	3.0	11460	124.3	79	3.3
9	$_S$**Z**	70	0.4	3.0	9290	122.4	81	4.3
10	$_S$**T**	40	0	0.4	1560	133.4	1512	3.5
11	$_S$**T**	60	0	1.0	3760	133.5	1636	2.7
12	$_S$**T**	60	0.2	0.7	2670	120.6	978	3.7
13	$_S$**T**	60	0.4	0.9	2250	118.7	686	4.1
14	$_S$**T**	70	0	1.2	3940	131.4	1487	3.2
15	$_S$**T**	70	0.2	0.5	2920	116.8	865	3.9
16	$_S$**T**	70	0.4	0.5	2440	116.1	600	4.2

Polymerization conditions: supported catalyst 20–30 mg, TMA 0.1 mmol solvent 150 mL hexane, ethylene pressure 150 psig, time 15 min.
[a] Mole ratio of 1-hexene/ethylene.
[b] Activity in kg PE/(mol Zr or Ti × h).

a continuous ethylene flow to meet the 150 psig at a stirring rate of 500 rpm. At the end of the polymerization, the reactor was rapidly vented and the obtained polymer was precipitated and washed with acidified (2 wt.% hydrochloric acid) ethanol, filtered, and dried under vacuum.

2.5. Polymer characterization

The catalyst activity was calculated as the mass of polymer product divided by the number of moles of metal (Zr, Ti, Ni) per hour. The melting temperature (T_m) of the obtained polymer was measured by differential scanning calorimeter (DSC, TA Instruments Q2000). The second scan was done at a heating rate of 10 °C/min and used to characterize the sample. Molecular weight averages (M_w), distributions (MWD) and SCB across MWD were determined by gel permeation chromatography with an infrared spectroscopy detector (GPC-IR, Polymer Char). Samples were dissolved at 145 °C with 1,2,4-trichlorobenzene and passed through three linear polymer laboratories columns which were calibrated with polystyrene standards and operated with a flow rate of 1 mL/min. The CCD was measured with crystallization elution fractionation (CEF, Polymer Char). Samples were dissolved at 160 °C for 60 min, followed by 5 min of equilibration at 95 °C. The cooling rate during crystallization was 3 °C/min, from 95 to 35 °C, and then the heating rate during elution was 3 °C/min, from 35 to 140 °C with 1 mL/min elution flow. The SCB frequency was analyzed by ^{13}C NMR spectroscopy (Varian Inova-500 NMR). The polymer was first made into a film using a hot press and was cut about 4.2 cm × 0.3 cm. A sample mass of 0.1 g and 0.7 g of tetrachloroethane-d_2 solvent were transferred into the 5 mm NMR tube, and the sample was allowed to dissolve at 130 °C. The operation was made with 120 °C with 2000 scanning number. Scanning electron microscopy (SEM, Leo Electron Microscopy LEO 1530) analysis was used to investigate the polymer particle morphology.

3. Results and discussion

3.1. Supported catalyst structure

Scheme 1 shows the proposed structures for the supported hybrid catalysts, including the borate activator. The metallocenes (**Z** and **T**) with functional *t*-butoxy groups, and the nickel diimine catalyst (**N**) with functional amine groups, are likely to be covalently attached onto the TMA-treated SiO_2-support. These chemical bonds strongly tether the catalysts onto the SiO_2 surface, resulting in minimal active site leaching during polymerization. The borate, which is used in stoichiometric ratio to activate the catalyst, is physisorbed onto the SiO_2-support. These pre-activated supported catalysts avoid costly process modification for external activator supply and elimination [17]. In addition, they enhance the polymer particle morphology by reducing reactor fouling that happens

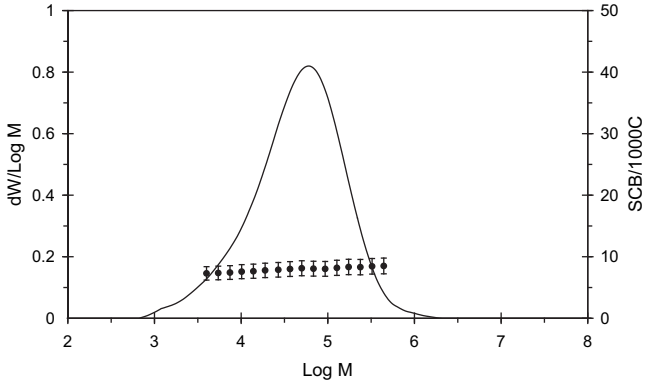

Fig. 2. MWD and SCB frequency profiles of poly(ethylene-*co*-1-hexene) made with $_S$**Z** (Run 9, Table 2).

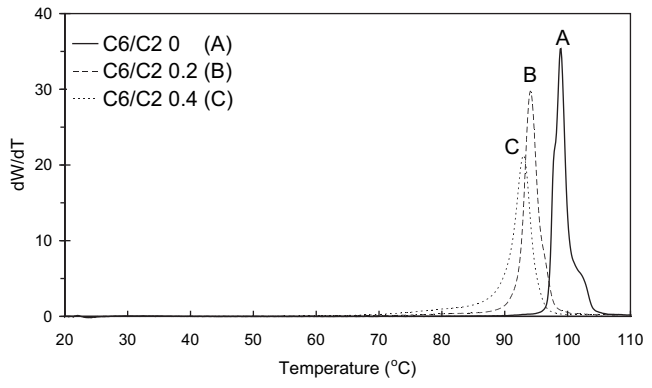

Fig. 3. CEF (CCD) profiles of poly(ethylene-*co*-1-hexene) made with $_S$**Z**: A (Run 7, Table 2), B (Run 8, Table 2) and C (Run 9, Table 2).

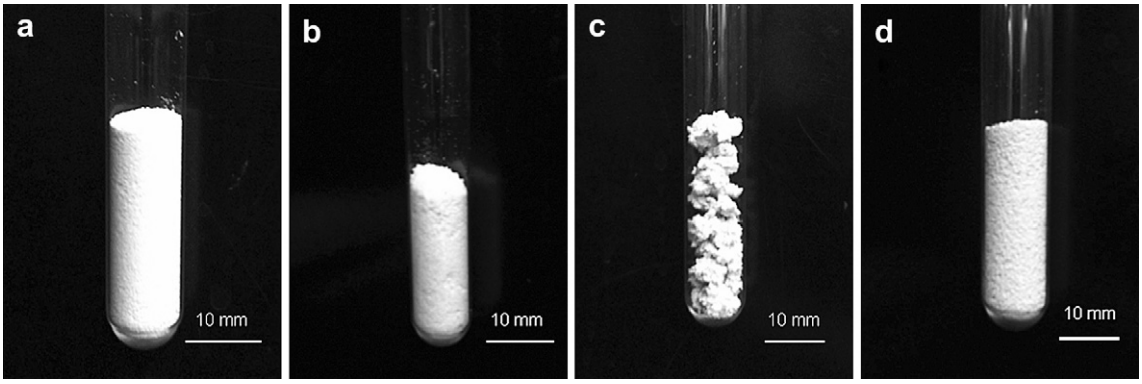

Fig. 4. Representative pictures of polymer particles made with a: $_S$**Z** (Run 9, Table 2), b: $_S$**T** (Run 14, Table 2), c: $_S$**T** (Run 16, Table 2), and d: $_S$**N** (Run 9, Table 3).

Table 3
Results for ethylene homopolymerization and ethylene/1-hexene copolymerization with $_S$**N**.

Run	Polymerization Conditions			Results				
	Catalyst	Temperature (°C)	1-Hexene (C6/C2)[a]	Yield (g)	Activity[b]	T_m (°C)	M_w (g/mol × 10^{-3})	M_w/M_n
1	$_S$**N**	40	0	1.7	6810	128.5	98	3.7
2	$_S$**N**	40	0.2	1.7	6230	127.5	85	4.2
3	$_S$**N**	40	0.4	1.9	6940	126.6	87	4.3
4	$_S$**N**	60	0	4.0	16200	125.4	96	4.2
5	$_S$**N**	60	0.2	3.4	13670	124.3	73	4.7
6	$_S$**N**	60	0.4	3.6	11550	123.6	66	4.1
7	$_S$**N**	70	0	2.4	9610	123.0	86	4.1
8	$_S$**N**	70	0.2	2.1	6500	121.9	61	4.2
9	$_S$**N**	70	0.4	1.2	4140	121.3	67	4.5

Polymerization conditions: supported catalyst 20–30 mg, TMA 0.1 mmol solvent 150 mL hexane, ethylene pressure 150 psig, time 15 min.
[a] Mole ratio of 1-hexene/ethylene.
[b] Activity in kg PE/(mol Ni × h).

when abstracted catalyst molecules become active for polymerization by reaction with activator present in solution.

Table 1 summarizes the components and the ICP results of all supported catalysts. Most of the catalyst metal components were deposited onto the SiO_2-support, but supporting efficiencies for Al were much lower. Alkyl aluminum molecules are expected to first react with the hydroxyl groups available on the SiO_2-support and the remaining excess molecules are then physically adsorbed onto the surface.

3.2. Ethylene polymerization

3.2.1. Supported single catalysts ($_S$**Z**, $_S$**T**, $_S$**N**)

Ethylene homopolymerization and copolymerization with 1-hexene using $_S$**Z** and $_S$**T** were conducted under various polymerization

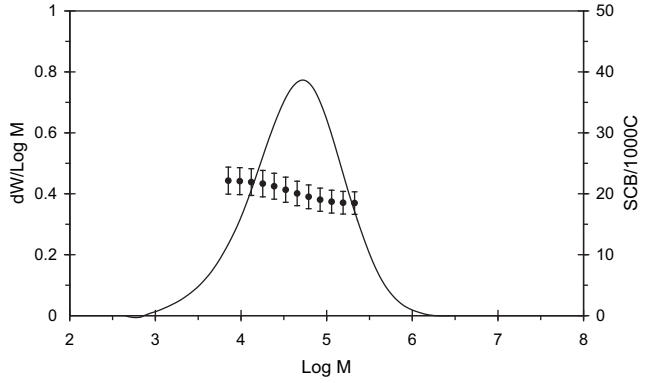

Fig. 5. MWD and SCB frequency profiles of polyethylene made with $_S$**N** (Run 7, Table 3).

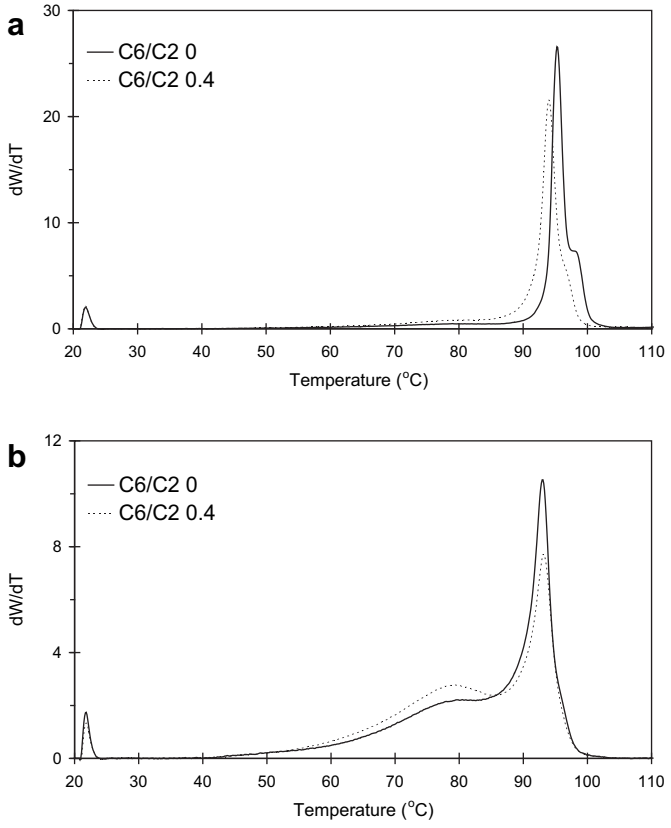

Fig. 6. CEF profiles for poly(ethylene-*co*-1-hexene) made with $_S$**N**: a) (Run 1 and 3, Table 3) and b) (Run 7 and 9, Table 3).

Table 4
Results for ethylene homopolymerization and ethylene/1-hexene copolymerization with $_{S}$**ZN**.

Run	Polymerization Conditions			Results				
	Catalyst	Temperature (°C)	1-Hexene (C6/C2) [a]	Yield (g)	Activity[b]	T_m (°C)	M_w (g/mol × 10^{-3})	M_w/M_n
1	$_{S}$**ZN**	40	0	1.0	4300	130.1	206	6.2
2	$_{S}$**ZN**	40	0.2	1.1	4110	128.1	141	5.5
3	$_{S}$**ZN**	40	0.4	1.0	4150	126.1	136	6.2
4	$_{S}$**ZN**	60	0	3.3	13260	128.7	124	7.1
5	$_{S}$**ZN**	60	0.2	2.6	10430	124.7	83	6.0
6	$_{S}$**ZN**	60	0.4	1.9	6120	122.5	96	7.8
7	$_{S}$**ZN**	70	0	3.7	14160	130.6	131	7.1
8	$_{S}$**ZN**	70	0.1	2.4	8710	125.5	106	5.1
9	$_{S}$**ZN**	70	0.2	1.7	6870	123.9	100	4.6
10	$_{S}$**ZN**	70	0.4	1.1	6440	120.2	77	6.4

Polymerization conditions: supported catalyst 20–30 mg, TMA 0.1 mmol solvent 150 mL hexane, ethylene pressure 150 psig, time 15 min.
[a] Mole ratio of 1-hexene/ethylene.
[b] Activity in kg PE/(mol Zr and Ni × h).

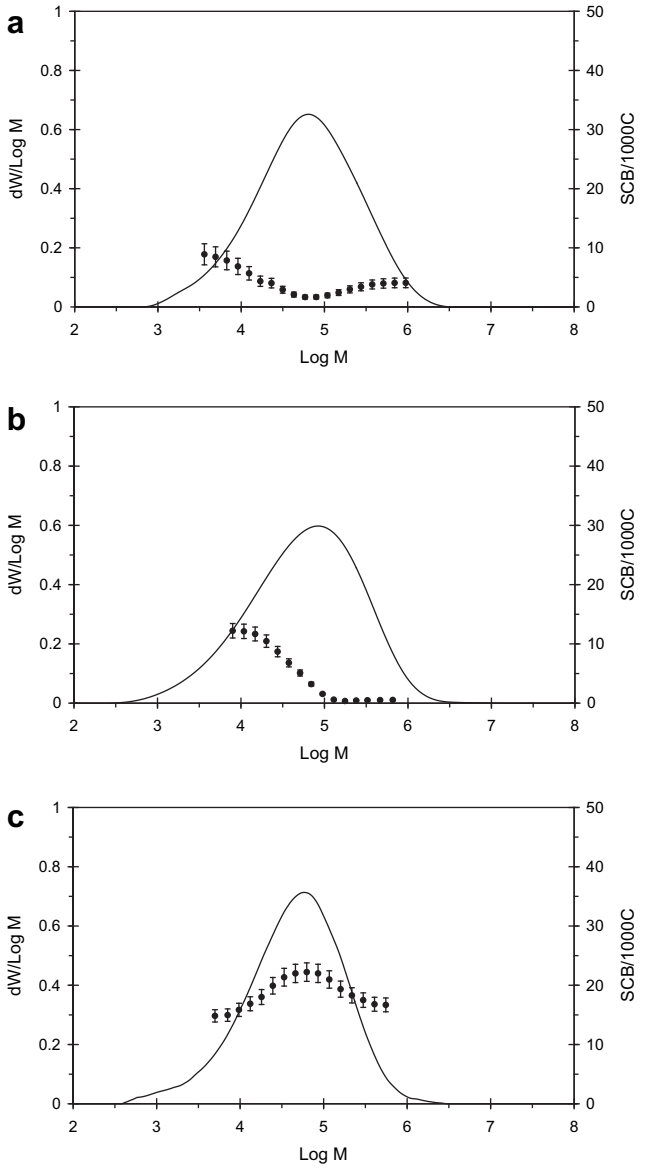

Fig. 7. MWD and SCB frequency of polyethylene made with $_{S}$**ZN**. Polymerization conditions: a) 40 °C, C6/C2 0.4 (Run 3, Table 4); b) 70 °C, C6/C2 0 (Run 7, Table 4); c) 70 °C, C6/C2 0.4 (Run 10, Table 4).

conditions (Table 2). The catalyst activity is higher at higher temperatures, but decreases with increased 1-hexene concentration in the reactor. Increasing temperature or increasing 1-hexene concentration leads to polymer with lower M_w. $_{S}$**T** made polymer with higher M_w than $_{S}$**Z**, but the catalyst activity is much lower than that of $_{S}$**Z**. As expected, the T_m of the polymer was proportional to 1-hexene reactor concentration, and this effect is more pronounced at higher temperatures. $_{S}$**T** made polymer with lower T_m than $_{S}$**Z** under the same conditions, indicating that **T** is more reactive towards α-olefin incorporation due to its constrained geometric ligand structure [19].

Fig. 2 shows the GPC-IR plot for an ethylene and 1-hexene copolymerization using $_{S}$**Z** (Run 9, Table 2). The SCB frequency across the MWD is practically the same; this is a well-known characteristic of copolymers made with metallocenes and other single-site catalysts, as opposed to heterogeneous Ziegler–Natta polymers [20].

Comparative CEF results for copolymers made with $_{S}$**Z** at 70 °C with different 1-hexene concentrations are shown in Fig. 3. CEF is a new technique that achieves excellent fractionation results based on the crystallizabilities copolymer chains in solution, combines aspects of crystallization analysis fractionation (CRYSTAF) and temperature rising elution crystallization (TREF) [21]. In the CEF profiles shown in Fig. 3, as the 1-hexene concentration in the reactor increases, the CCD peak shifts to lower temperatures (A: 99.0 °C; B: 94.2 °C; C: 93.2 °C), indicating higher 1-hexene incorporation in the copolymer. The high crystallization temperature peak shown for the homopolymer sample A is related to crystallization kinetics in CEF and should not be interpreted as differences in 1-hexene content, which is nil for this particular sample.

For the ethylene slurry polymerization, all polymer particles were obtained in the form of free-flowing powders, except one sample made with $_{S}$**T** with high 1-hexene content (Run 16, Table 2). Representative pictures of polymer particles are shown Fig. 4. The samples were transferred to round bottom glass tubes with 10 mm diameter that became filled with free-flowing polymer particles. This indicated that metallocenes **Z** and **T**, having *t*-butoxy functional groups, were strongly supported on SiO_2 through covalent chemical bonding without any apparent abstraction of active sites during polymerization, resulting excellent polymer particle morphologies (the so-called replication phenomenon) [22]. Moreover, these long alkyl groups bonding support and active site might provide enough space to reduce steric hindrance between the bulky SiO_2 surface and the active sites, thus favoring high catalyst activity. The copolymer with the high α-olefin incorporation was the only exception to the rule (Fig. 4.c), not because of site extraction, but due to the low crystallinity, "sticky"copolymer made during this copolymerization which led to particle agglomeration.

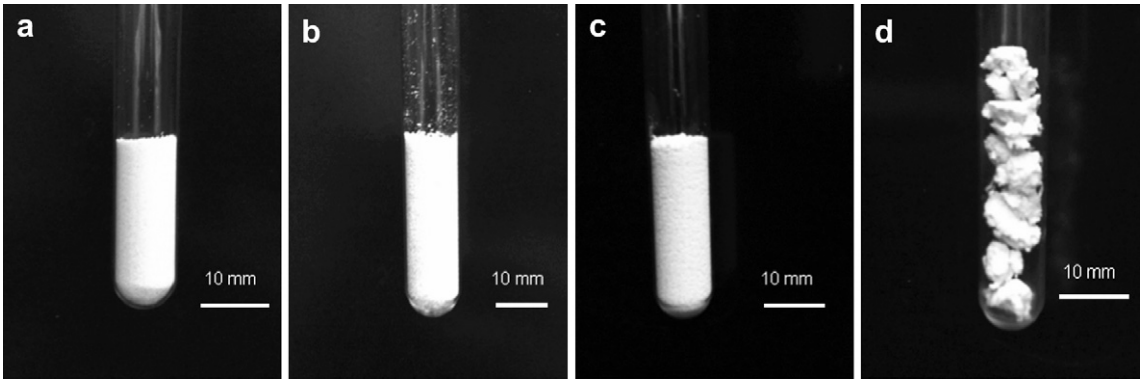

Fig. 8. Representative pictures of polymer particles made with a: $_S$**ZN** (Run 10, Table 4), b: $_S$**TN** (Run 3, Table 6), c: $_S$**TN** (Run 7, Table 6), and d: $_S$**TN** (Run 9, Table 6).

Table 3 shows the polymerization results using $_S$**N**. In contrast to $_S$**Z** and $_S$**T**, the activities of $_S$**N** are the highest at 60 °C. The catalyst activity for $_S$**N** is higher than for $_S$**Z** and $_S$**T** at the same 1-hexene concentration at 40 °C and 60 °C. $_S$**N** made polymer with lower M_w, and slightly broader MWD than $_S$**Z** and $_S$**T**. It seems that the 1-hexene concentration does not affect much the catalyst activity and the T_m of the polymer. Higher temperatures, however, leads to polymers with lower T_m by increasing the frequency of SCB formed by the chain walking mechanism [23]. The low α-olefin reactivity of the nickel diimine catalyst is partially caused by active sites that are sterically hindered by bulky ligands, which limits α-olefin insertion onto the growing polymer chain. At the same time, these ligands make it possible to produce polymer with high M_w by depressing chain transfer reaction [24,25].

Fig. 5 shows the GPC-IR plot for the ethylene homopolymer made with $_S$**N**. The SCB frequency across the MWD decreases slightly at the highest molecular weights. Theoretically the SCB profile should be flat as well. This is probably some non-ideal behavior of the supported catalyst, or may be some GPC-related issues. More highly branched chains are more compact in solution, and therefore elute at lower elution volumes and are "perceived" by the calibration curve as having higher molecular weights.

The CEF profiles in Fig. 6.a show that narrow peaks are obtained for polymers made at 40 °C; they are similar to those made with $_S$**Z**, as shown in Fig. 3. Addition of 1-hexene shifts the CEF peak temperature from 95.4 to 94.1 °C (compare with Fig. 3, where a much more pronounced change is observed when $_S$**Z** is used). Interestingly, the CEF profiles for polymers made at 70 °C (Fig. 6.b) have two well-defined peaks (93.2 °C and 79.0 °C), regardless of the 1-hexene concentration that varies slightly in relative amount as the concentration of 1-hexene in the reactor changes. These results are unusual, since $_S$**N** was expected to make polymers with unimodal SCBD due to its single-site nature; however, the CEF profiles look like those of LLDPE made with multiple-site systems such as heterogeneous Ziegler–Natta catalysts. As shown in Fig. 4.d, this bimodality is not caused by the partial extraction of active sites out of the SiO_2-support, since free-flowing, high bulk density particle are produced during polymerization. Instead, it is likely that the supported nickel diimine catalyst $_S$**N** has at least two types of active sites that depend on specific site environments such as different configurations or locations on the SiO_2-support. One active site type seems to be more prone to chain walking and makes polymer with lower CEF elution temperatures (79 °C) at the higher polymerization temperature of 70 °C. This difference is not as apparent for polymers made at 40 °C (Fig. 6.a) because the chain walking frequency decreases significantly when the temperature is reduced.

3.3. *Supported hybrid catalysts ($_S$**ZN**, $_S$**TN**)*

Ethylene homopolymerization and ethylene/1-hexene copolymerization using $_S$**ZN** were conducted under the same polymerization conditions with supported single catalysts, and the results are summarized in Table 4. The catalyst activity, polymer T_m, and M_w fall between the values obtained for the single catalysts $_S$**Z** and $_S$**N**. As expected, all polymers have broader MWD than polymers made with supported single catalysts. Therefore, it seems that each active site type, **Z** and **N**, behaves independently of each other on the hybrid $_S$**ZN**.

The SCB frequency across the MWD is shown in Fig. 7. Two polymer populations are present in the overall resin: the lower

Table 5
Theoretically calculated catalyst activity and M_w for $_S$**ZN** using results for $_S$**Z** and $_S$**N**.

Entry	Polymerization Conditions			Results				
	Cat.	Temperature (°C)	1-hexene (C6/C2) [a]	(Z:N) [b]	Activity		M_w (g/mol × 10^{-3})	
					Calc.	Exp.	Calc.	Exp.
	$_S$**ZN**	40	0	32:68	5570	4300	189	206
2	$_S$**ZN**	40	0.2	25:75	5200	4110	126	141
3	$_S$**ZN**	40	0.4	23:77	5810	4150	116	136
4	$_S$**ZN**	60	0	41:59	14180	13260	130	124
5	$_S$**ZN**	60	0.2	36:64	11510	10430	95	83
6	$_S$**ZN**	60	0.4	29:71	9580	6120	79	96
7	$_S$**ZN**	70	0	65:35	14820	14160	128	131
8	$_S$**ZN**	70	0.2	64:36	9640	6870	73	100
9	$_S$**ZN**	70	0.4	69:31	7690	6440	80	77

[a] Mole ratio of 1-hexene/ethylene.
[b] Contributed mole fraction of **Z** and **N** on activity and M_w.

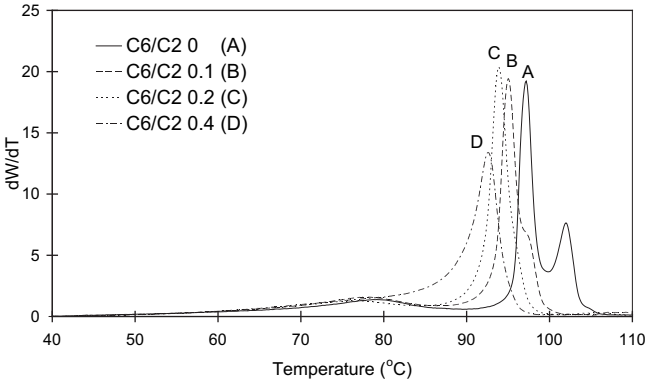

Fig. 9. CEF (CCD) profiles of polyethylene made with $_S$**ZN**: A (Run 7, Table 4), B (Run 8, Table 4), C (Run 9, Table 4) and D (Run 10, Table 4).

molecular weight population is made with the **N** catalyst and the high molecular weight polymer is made with the **Z** catalyst. The SCB frequency of the lower molecular weight polymer increases when the temperature changes from 40 to 70 °C (compare Fig. 7.a and.b) because the chain walking frequency for the **N** catalyst increases at higher temperatures. No SCBs are detected in the higher molecular weight population in absence of 1-hexene (Fig. 7.b), since SCBs are formed by 1-hexene incorporating by the **Z** catalyst. Accordingly, as the 1-hexene concentration in the reactor increases, the SCB frequency of the higher molecular weight population increases, becoming higher than that of the lower molecular weight polymer, as shown in Fig. 7.c.

Short chain branches of various lengths (but predominantly methyl SCBs) are made by chain walking in the lower molecular weight population, and their frequency can be controlled by changing the polymerization temperature. At the same time, the amount of butyl branches of the higher molecular weight population is easily controlled by 1-hexene addition to the reactor. Therefore, this novel polyolefin has a rather unique microstructure that can be controlled by 1-hexene concentration, polymerization temperature, and **N/Z** ratio to optimize the polymer microstructure for a particular application. Moreover, $_S$**ZN** makes polymer with broad MWD, good processability (as attested by $M_w/M_n > 4.5$), and free-flowing particles (Fig. 8.a) without reactor fouling.

To verify whether the **Z** and **N** catalysts behaved independently of each other in the $_S$**ZN** catalyst, we calculated the catalyst activity and M_w for $_S$**ZN** based on the values of $_S$**Z** and $_S$**N** at similar conditions. First, the molar fractions of polymer made with **Z** and **N**, m_Z and m_N, respectively, in the combined $_S$**ZN** catalyst were estimated using Equations (1) and (2),

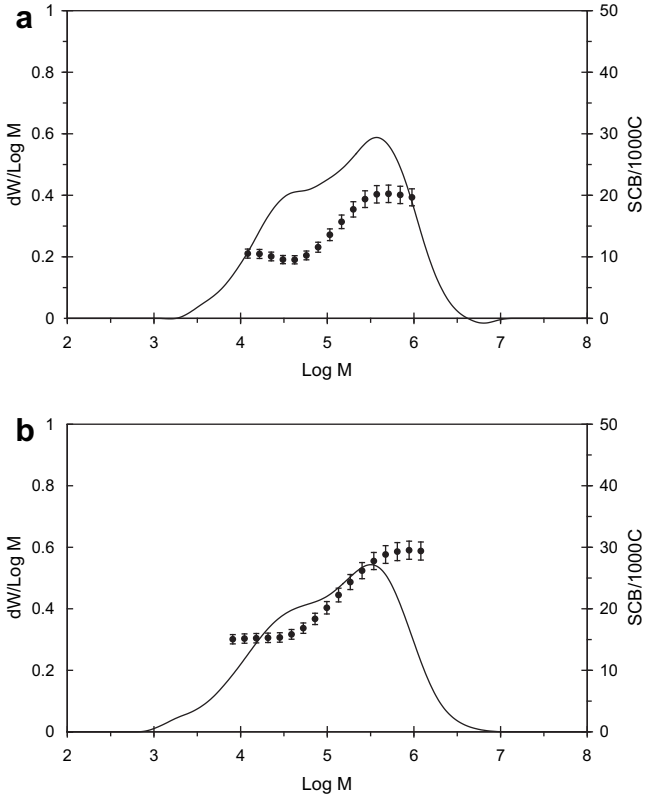

Fig. 10. MWD and SCB frequencies for polyethylene made with $_S$**TN**. Polymerization conditions: a) 40 °C, C6/C2 0.4 (Run 3, Table 6); b) 70 °C, C6/C2 0.4 (Run 9, Table 6).

$$m_Z = \frac{\text{Activity of the } \mathbf{Z} \text{ catalyst}}{\text{Combined activity of the} \mathbf{Z} \text{ and } \mathbf{N} \text{ catalysts}} = \frac{x_Z A_{S^Z}}{x_Z A_{S^Z} + x_N A_{S^N}} \quad (1)$$

$$m_N = 1 - m_Z \quad (2)$$

where x_Z and x_N are the molar fractions of **Z** and **N** in $_S$**ZN**, respectively, A_{S^Z} and A_{S^N} are the polymerization activities of **Z** and **N**, respectively, based on their activities when supported alone as $_S$**Z** and $_S$**N**.

For example, for Run 1 in Table 5,

$$m_Z = \frac{0.5 \times 3250}{0.5 \times 3250 + 0.5 \times 6810} = 0.32 \quad (3)$$

Table 6
Results for ethylene homopolymerization and ethylene/1-hexene copolymerization using $_S$**TN**.

Run	Polymerization Conditions			Results				
	Catalyst	Temperature (°C)	1-Hexene (C6/C2) [a]	Yield (g)	Activity[b]	T_m (°C)	M_w (g/mol × 10^{-3})	M_w/M_n
1	$_S$**TN**	40	0	0.5	800	131.0	633	19.1
2	$_S$**TN**	40	0.2	0.6	1000	124.5	351	7.5
3	$_S$**TN**	40	0.4	0.5	500	122.4	301	6.8
4	$_S$**TN**	60	0	1.5	2300	128.2	682	29.0
5	$_S$**TN**	60	0.2	1.2	1800	120.8	491	16.9
6	$_S$**TN**	60	0.4	1.4	1700	119.3	375	12.9
7	$_S$**TN**	70	0	1.8	2800	128.3	595	29.8
8	$_S$**TN**	70	0.2	1.5	2300	119.5	345	15.6
9	$_S$**TN**	70	0.4	1.2	1800	119.0	309	11.3

Polymerization conditions: supported catalyst 20–30 mg, TMA 0.1 mmol solvent 150 mL hexane, ethylene pressure 150 psig, time 15 min.
[a] Mole ratio of 1-hexene/ethylene.
[b] Activity in kg PE/(mol Ti and Ni × h).

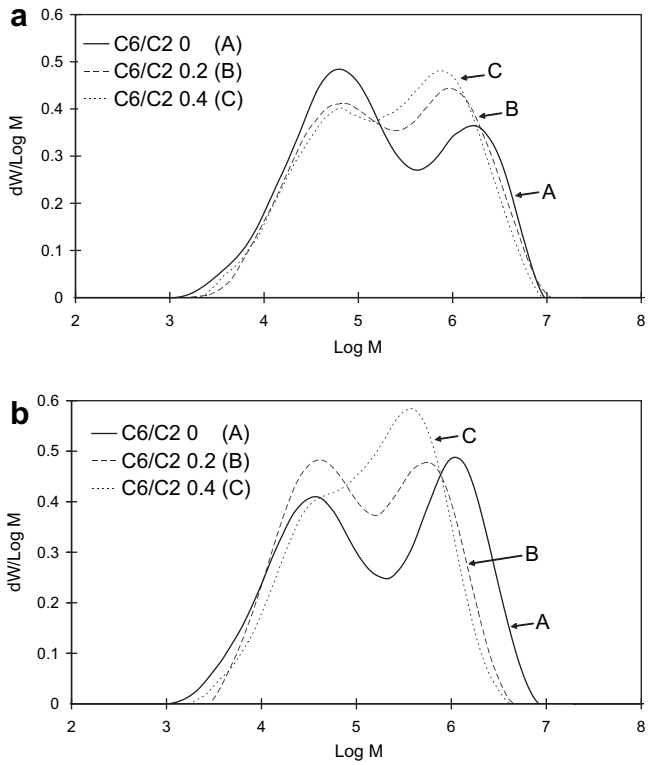

Fig. 11. Comparison of MWDs for polyethylene samples made with $_S$**TN** at: a) 40 °C (Runs 1–3, Table 6) and b) 70 °C (Runs 7–9, Table 6).

$$m_N = 1 - 0.32 = 0.68 \quad (4)$$

Overall catalyst activity$A_{S^{ZN}}$, and M_w for the whole polymer, $M_{w_{S^{ZN}}}$, were estimated using Equations (5) and (6)

$$A_{S^{ZN}} = m_Z A_{S^Z} + m_N A_{S^N} \quad (5)$$

$$Mw_{S^{ZN}} = m_Z M_{w_{S^Z}} + m_N M_{w_{S^N}} \quad (6)$$

Table 5 compares experimental and predicted catalyst activities and weight average molecular weights for the polymers made with the $_S$**ZN** catalyst. The experimental activities are slightly lower than the calculated results, while the experimental M_w are generally higher than the predicted values. However, considering batch-to-batch variations among the supported catalysts, and considering that the **N** and **Z** catalysts have different sensitivity to polar poisons that may be present on the support and in the reactor during polymerization, the agreement between predictions and experimental results is acceptable and indicates that the catalysts sites act independently in when co-supported on the same carrier.

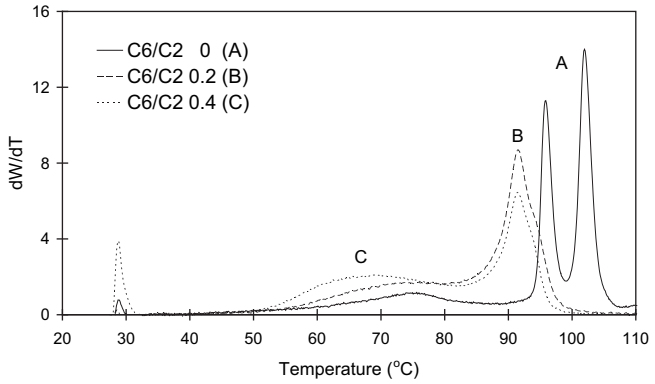

Fig. 12. CEF (CCD) profiles for polyethylene samples made with $_S$**TN**: A (Run 7, Table 6), B (Run 8, Table 6), C (Run 9, Table 6).

CEF analysis results are shown in Fig. 9. The CCD of the polymer made with $_S$**ZN** has unique characteristics. The homopolymer (no 1-hexene co-monomer added) has a trimodal CCD (A). The polymer in the high-crystallinity peak (102.1 °C) was made with the **Z** catalysts, and the polymer composing the other two peaks (97.2 °C and 79.7 °C) containing SCBs made via the chain walking mechanism was made by catalyst **N**. According to the theoretically calculated result in Entry 7 (Table 5), 65% of the polymer was made by **Z**. However, the area under the high-temperature peak in Fig. 10.A does not correspond to 65% of the total polymer. Although the position of the $_S$**ZN** peak with the lowest elution temperature (79.7 °C) coincides with that for the polymer made with $_S$**N** (compare with Fig. 6), the intermediate peak (97.2 °C) is shifted to a higher temperature. This shift indicates that co-crystallization takes place between the high-crystallinity component made by **N** and the polymer made by **Z**, as co-crystallization phenomena is commonly observed, especially for peaks with similar high crystallizabilities, in this types of analytical techniques.

The **Z** active sites incorporate more α-olefin than the **N** sites. As a consequence, the CEF elution temperature of polymer made with **Z** decreases much more significantly as the 1-hexene concentration in the reactor increases. Observing how the two highest elution temperature peaks vary from A to D in Fig. 9, we notice that the

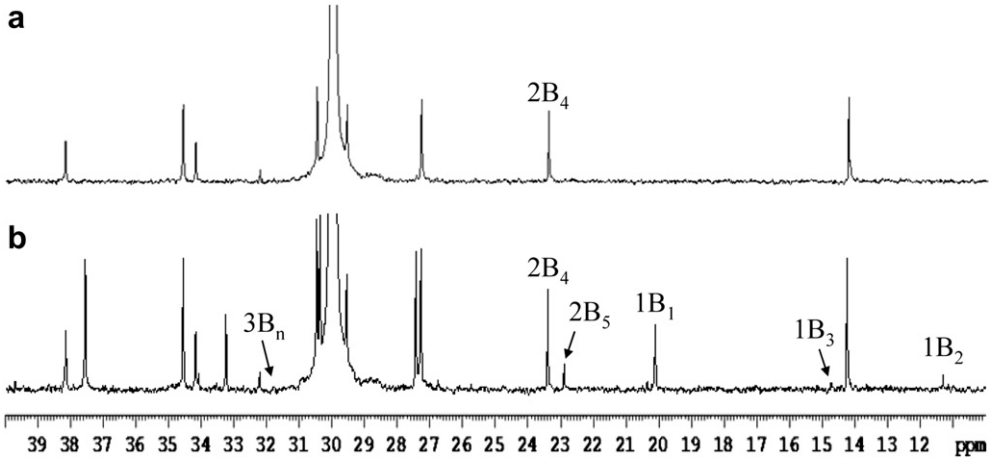

Fig. 13. High-temperature ^{13}C-NMR spectra for polyethylenes made with: a) $_S$**Z** (Run 9, Table 2), and b) $_S$**ZN** (Run 10, Table 4).

Table 7
Influence of catalyst structures and polymerization conditions on SCBD.

Entry	Polymerization Conditions			SCBs/1000C	SCBD (%)					
	Catalyst	Temperature (°C)	1-hexene (C6/C2)[a]		Methyl	Ethyl	Propyl	Butyl	Pentyl	($n \geq 6$)
1	$_S$**Z**	70	0.4	7.33	0	0	0	100	0	0
2	$_S$**N**	70	0.4	27.65	55.9	10.0	8.0	14.4	6.3	5.4
3	$_S$**ZN**	40	0.4	4.48	84.0	0	0	16.0	0	0
4	$_S$**ZN**	70	0	11.38	65.2	11.0	6.2	5.4	5.1	7.1
5	$_S$**ZN**	70	0.4	16.24	29.9	6.2	4.5	42.2	9.5	7.7
6	$_S$**TN**	40	0.4	14.84	25.9	0	0	74.1	0	0
7	$_S$**TN**	70	0	8.23	51.8	7.1	8.2	12.9	7.1	12.9
8	$_S$**TN**	70	0.4	28.13	13.0	2.3	2.1	71.1	4.9	6.6

[a] Mole ratio of 1-hexene/ethylene.

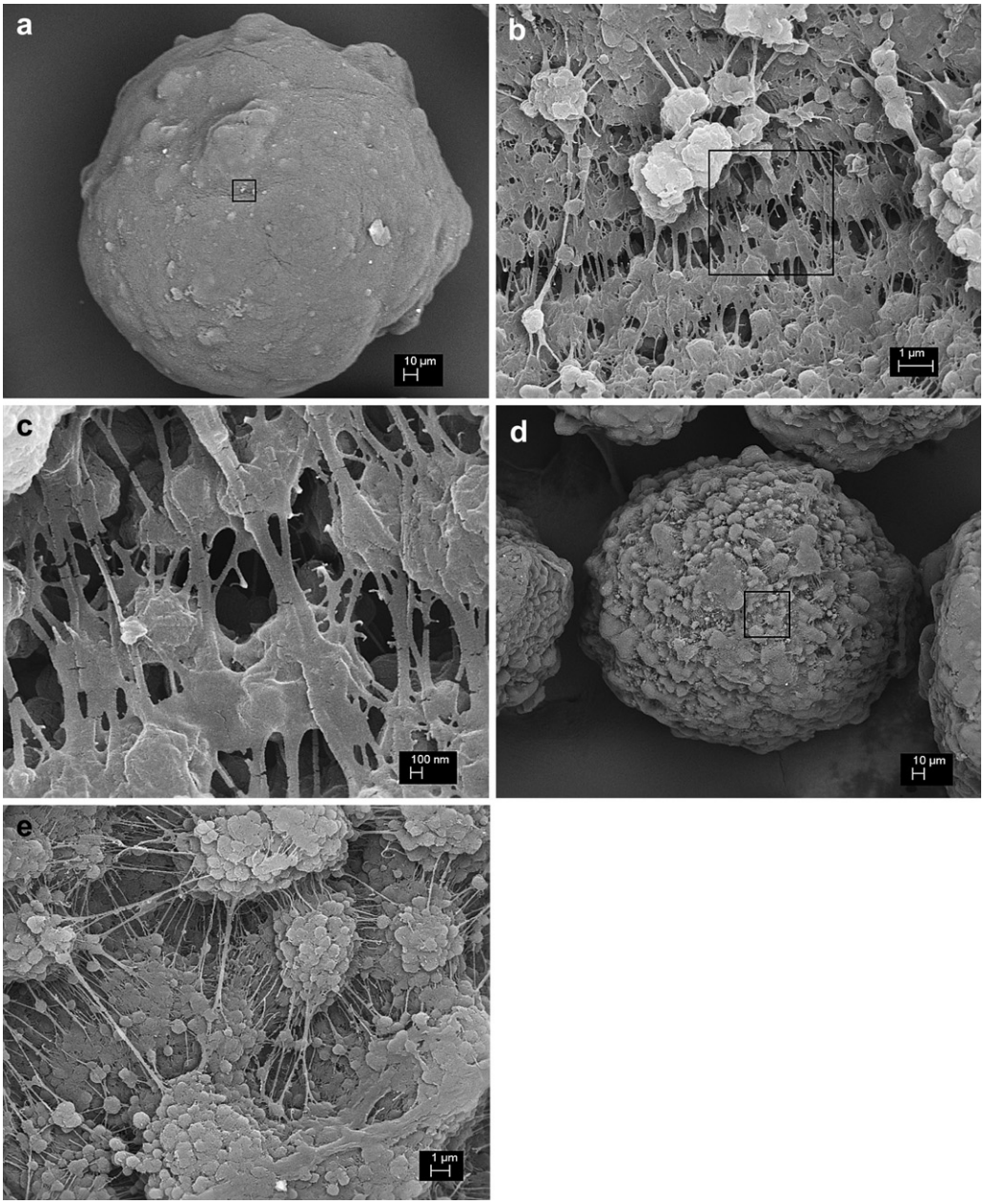

Fig. 14. SEM micrographs of polymer particles made with $_S$**ZN** (Run 7, Table 4): a) external surface (scale bar 10 µm); b) A closer look at the region indicated with a square box on a) (scale bar 1 µm); c) A closer look at the region indicated with a square box on b) (scale bar 100 nm); d) particle with different morphology from a) (scale bar 10 µm); e) A closer look at the region indicated with a square box on d) (scale bar 1 µm).

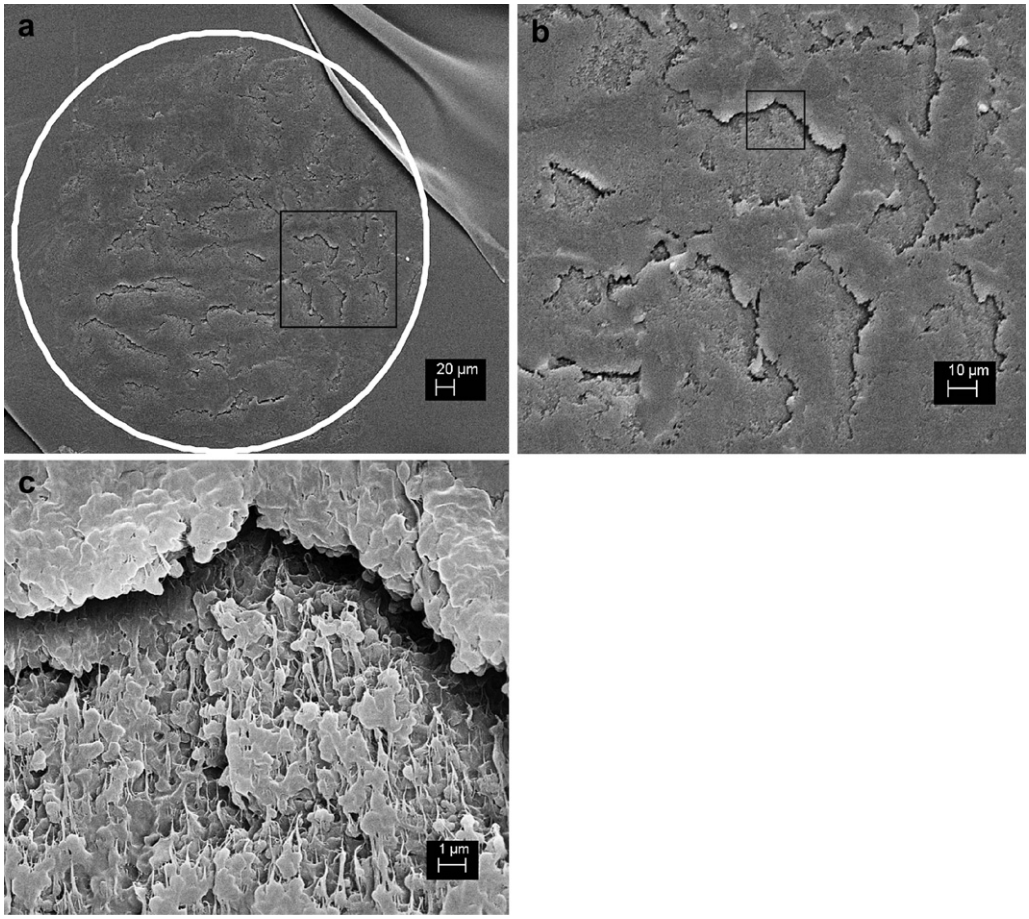

Fig. 15. SEM micrographs of a microtomed slice of a polymer particle made with $_S$**ZN** (Run 7, Table 4): a) a sliced particle (inside white circle, scale bar 20 μm); b) A closer look at the region indicated with a square box on a) (scale bar 10 μm); c) A closer look at the region indicated with a square box on b) (scale bar 1 μm).

peak attributed to **Z**, initially appears well resolved in A, becomes a shoulder of the **N** peak in B, completely overlaps the **N** peak in C, and finally seems to "appear" again at a lower elution temperature in D. Interestingly, the peak located at 80 °C, also attributed to catalyst **N**, hardly changes in size or shape as 1-hexene concentration is increased. This indicated that most, if not all, of the SCBs are caused by chain walking and are not affected by the presence of 1-hexene during the polymerization. Based on these CEF results, we may hypothesize the presence of at least three kinds of active sites on $_S$**ZN**, each with its own characteristics and contributing to make polyethylene with unique microstructural properties.

Results for ethylene polymerizations using $_S$**TN** are shown in the Table 6. The catalyst activity and T_m of polymer are lower than for polymers made with $_S$**ZN** in the same polymerization condition. On the other hand, $_S$**TN** made polymers with higher M_w and broader, bimodal MWDs due to the presence of the **T** sites. As seen from the GPC-IR results in Fig. 10, polymers with bimodal MWD and reverse co-monomer incorporation can be made with this hybrid catalyst. A high amount of SCBs were incorporated in the higher molecular weight region of the distribution, resulting in polymer with inverse SCBD even at 40 °C (Run 3, Table 6, and Fig. 10.a). At higher polymerization temperatures (70 °C), the polymer becomes even more branched (Fig. 10.b).

Fig. 11 shows various MWD profiles of polymer made using $_S$**TN**. As the concentration of 1-hexene increases, the area under the peak corresponding to catalyst **T** increases and gradually shifted to lower molecular weight averages, but the peak location for the **N** catalyst does not change appreciably. The **T** active sites have higher reactivity ratio towards 1-hexene incorporation, and therefore the relative mass of polymer made on these sites increases and the concentration of 1-hexene is raised; however, due to transfer to co-monomer, the molecular weight distribution for polymer made on these sites also decreases. Site **N**, with a much lower 1-hexene incorporation ratio, is not significantly affected by the presence of the α-olefin co-monomer. Thus, the MWD becomes narrower with increasing 1-hexene concentrations. Most of polymers are free-flowing particles, but the polymers with the highest 1-hexene feed at 70 °C are agglomerated, as seen in Fig. 8.d.

Fig. 12 shows the CEF results for the polymers made with $_S$**TN**. The CCD for the homopolymer (A) is similar to that for $_S$**ZN**. The polymer with the highest elution peak (102.1 °C) is made on the **T** sites (compare with CEF for polymers made with $_S$**Z**, Fig. 3). The other two peaks at lower temperatures are for polymer made with the **N** catalyst. Adding 1-hexene to the reactor makes the peak with the highest co-monomer incorporation ability (**T**) move the lower temperatures, while the peaks corresponding the **N** catalyst are less affected, similarly to what had been observed for copolymer made with the $_S$**ZN** system.

3.4. SCB characterization

The SCB distribution was further characterized by ^{13}C NMR spectroscopy. The assignments of each characteristic chemical shifts at 20.15(1$\mathbf{B}_1$), 11.32(1$\mathbf{B}_2$), 14.75(1$\mathbf{B}_3$), 23.42(2$\mathbf{B}_4$), 22.92(2$\mathbf{B}_5$) and 31.77(3$\mathbf{B}_n$) for the resultant polymers are based on chemical shift calculations according to the Lindeman and Adams method

[26]. Representative ^{13}C NMR results are shown in Fig. 13. Equations used to calculate SCB/1000 C atoms and their relative ratios are given by the expressions [27],

$$N(\text{total branches}/1000C) = \frac{1000\left(I_{Me}/0.90 + I_{Et}/0.84 + I_{Pr}/0.83 + I_{Bu}/0.90 + I_{Pe}/0/90 + I_{Lg}/0.8\right)}{I_{main} + 5.5(I_{Et}/0.84) + I_{Pr}/0.83 + 8.0\left(I_{Bu}/0.90 + I_{Pe}/0/90 + I_{Lg}/0.8\right)} \quad (7)$$

$$\text{Me} : \text{Et} : \text{Pr}: \text{Pe} : \text{Lg} = (I_{Me}/0.90): (I_{Et}/0.84): (I_{Pr}/0.83): (I_{Bu}/0.90): (I_{Pe}/0.90): (I_{Lg}/0.80) \quad (8)$$

where, I_{Me}, I_{Et}, I_{Pr}, I_{Bu}, I_{Pe} and I_{Lg} are the ^{13}C NMR integral intensities corresponding to $1\mathbf{B}_1$, $1\mathbf{B}_2$, $1\mathbf{B}_3$, $2\mathbf{B}_4$, $2\mathbf{B}_5$ and $3\mathbf{B}_n$, respectively.

Table 7 shows the SCB distribution of some polymers synthesized in this study. The catalyst $_S$**N** make highly branched polymers with a distribution of SCB lengths, as characteristic of the chain walking mechanism. Methyl branches predominate, but 1-hexene incorporation onto the polymer chains is much lower than that for $_S$**Z** (Entries 1 and 2, Table 7), as already observed in the several CEF profiles discussed above. The SCBs of polymers made with $_S$**ZN** are intermediate between the results for polymers made with $_S$**Z** and $_S$**N** (Entries 1, 2 and 5, Table 7), as expected. The $_S$**TN** catalyst makes chains with the largest SCB frequency, due to the high co-monomer incorporation rate of the **T** component. As expected, butyl branches are mostly controlled by the contribution of the metallocene component (**Z** or **T**), while **N** adds an additional component with a distribution of SCB lengths, but mostly methyl branches. When **Z** is replaced with **T**, polyethylene with the highest butyl branch frequency is obtained for a given set of polymerization conditions (Runs 5 and 8, Table 7). In addition, the amount and types of SCBs can be modified by changing the polymerization temperature (Runs 3 and 5, Runs 6 and 8, Table 7).

3.5. Polymer morphology

SEM micrographs of polymer particles made with $_S$**ZN** (Run 7, Table 4) are shown in Fig. 14. Two distinct particle morphologies are observed as illustrated in Fig. 14.a (around 80% of total particles) and Fig. 14 d (around 20% of total particles). In Fig. 14.a, the polymer particle has a smooth surface and apparent high bulk density, while in Fig. 14.b the particle appears more porous. Fig. 14.b and c show zoom into a particular section of the particle, as indicated by the square box in Fig. 14.a. The primary particles (also called microparticles or sub-particles) consist of round fragments with diameters below 1 μm, and are connected through polymer fibrils. According to multigrain model, the secondary particle (also called macroparticle or polymer particle) is constituted by an agglomerate of near spherical primary particles, each containing a catalyst/support grain at its center [28,29].

Polymer particles with the morphology shown in Fig. 14.d were embedded in an epoxy resin and cut into slices with 15 μm thicknesses with a diamond knife. Fig. 15.a shows the SEM micrograph of such a slice (within the white circle). Fig. 15.b zooms in the square box depicted in Fig. 15.a. Irregular cluster shapes of 10–20 μm diameter replicate the external morphology shown in Fig. 14.e. The region indicated by a square box in Fig. 15.b is seen in higher magnification in Fig. 15.c, showing that some of the observed clusters have slightly different morphologies. The polymer shown in the upper part of the figure looks denser, and polymer fibrils are not observed. On the other hands, polymer fibrils are seen at the lower portion of the figure, which also looks less dense. This may be caused by non-uniform distribution of catalyst **Z** and **N** in the polymer particle, for instance.

4. Conclusions

Functionalized early transition metal and late transition metal catalysts were supported onto SiO_2 and used for ethylene homopolymerization and ethylene/1-hexene copolymerization. GPC-IR and CEF results revealed that when these catalysts were co-supported, they behaved independently of each other. The hybrid supported catalyst systems were very effective for the tailoring the polyethylene microstructure. Polymers with distribution SCB lengths were produced without addition of α-olefin by the nickel diimine catalyst via the chain walking mechanism, while the metallocene component needed α-olefin to produce branched chains. The combination of the **Z**, **T** and **Z** catalysts having unique characteristics led to polymers having broad and bimodal MWD and trimodal CCD. Depending on the polymerization conditions, an inverse distribution of SCBs across the MWD could be obtained, where the SCB frequency increases with increasing molecular weight.

The formation of free-flowing polymer particles confirms that the catalyst sites were strongly supported onto SiO_2. Furthermore, SEM micrographs showed that the polymer particles had spherical morphology and apparent high bulk density. Thus, these hybrid catalysts seem to be adequate for “drop-in” operations and may be used directly in most commercially available slurry or gas-phase process.

References

[1] Shan CLP, Soares JBP, Penlidis A. Polymer 2002;43:7345–65.
[2] Böhm LL. Angrew Chem Int Ed 2003;42:5010–30.
[3] Hong SC, Mihan S, Lilge D, Delux L, Rief U. Polym Eng Sci 2007;47:131–9.
[4] Soares JBP, Kim JD. J Polym Sci A Polym Chem 2000;38:1408–16.
[5] Mckenna TFL, Soares JBP. Chem Eng Sci 2001;56:3931–49.
[6] Hlatky GG. Chem Rev 2000;100:1347–76.
[7] Alonso C, Antiñolo A, Hermosilla FC, Carrión P, Otero A, Sancho J, et al. J Mol Catal A Chem 2004;220:286–96.
[8] Fink G, Steinmetz B, Zechlin J, Przybyla C, Tesche B. Chem Rev 2000;100:1377–90.
[9] Chu KJ, Soares JBP, Penlidis A. J Polym Sci A Polym Chem 2000;38:462–8.
[10] US 4701432 (1987) Exxon Chemical Patents Inc., inv.: H.C. Welborn, Jr.
[11] WO 982128 (1998) LG Chem., invs.: J.S. Oh, T.H. Park, B.Y. Park.
[12] Lee DH, Shin SY, Lee DH. Macromol Symp 1995;97:195–200.
[13] Dubois LH, Zegarski BR. J Am Chem Soc 1993;115:1190–1.
[14] EP 839836 (1997) Repsol, invs.: A.M. Lafuente, P.L. Canas, J.S. Royo, B.P. Garcia, M.F.M. Nunez, C.M. Marcos.
[15] Lee DH, Lee HB, Noh SK, Song BK, Hong SM. J Appl Polym Sci 1999;71:1071–80.
[16] US 7294600 (2007) LG Chem., invs.: K.S. Lee, H.S. Lee, E.J. Lee, S.W. Lee, C.H. Lee.
[17] Choi Y, Soares JBP. Macromol Chem Phys 2009;210:1979–88.
[18] Preishuber-Pflugl P, Brookhart M. Macromolecules 2002;35:6074–6.
[19] Mehdiabadi S, Soares JBP. Macromol Symp 2008;285:101–14.
[20] Bubeck RA. Mat Sci Eng 2002;39:1–28.
[21] Monrabal B, Sancho-Tello J, Mayo N, Romero L. Macromol Symp 2007;257:71–9.
[22] Abbenhuis HCL. Angew Chem Int Ed 1999;38:1058–60.

[23] Gate DP, Svejda SA, Onate E, Killian CM, Johnson LK, White PS, et al. Macromolecules 2000;33:2320–34.
[24] Johnson LK, Killian CM, Brookhart M. J Am Chem Soc 1995;117:6414–5.
[25] Schrekker HS, Kotov V, Pflugl PP, White P, Brookhart M. Macromolecules 2006;39:6341–54.
[26] Lindeman LP, Adams JQ. Anal Chem 1971;43:1245–52.
[27] Usami T, Takayama S. Macromolecules 1984;17:1756–61.
[28] Nagel EJ, Kirilov VA, Ray WH. Ind Eng Chem Prod Res Dev 1980;19:372–9.
[29] Mckenna TFL, Martino AD, Weickert G, Soares JBP. Macromol React Eng 2010;4:40–64.